JGR Oceans

RESEARCH ARTICLE
10.1029/2019JC015153

Effects of Swell Waves on Atmospheric Boundary Layer Turbulence: A Low Wind Field Study

Zhongshui Zou[1,2], Jinbao Song[1], Peiliang Li[1], Jian Huang[3], Jun A. Zhang[4,5], Zhanhong Wan[1], and Shuiqing Li[6,7,8]

[1]Ocean College, Zhejiang University, Zhoushan, China, [2]Ocean Research Center of Zhou Shan, Zhejiang University, Zhoushan, China, [3]Guangzhou Institute of Tropical and Marine Meteorology, CMA, Guangdong, China, [4]Cooperative Institute for Marine and Atmospheric Studies, University of Miami, Miami, FL, USA, [5]Hurricane Research Division, AOML, NOAA, Miami, Florida, USA, [6]Key Laboratory of Ocean Circulation and Waves, Institute of Oceanology, Chinese Academy of Sciences, Qingdao, China, [7]Laboratory for Ocean and Climate Dynamics, Qingdao National Laboratory for Marine Science and Technology, Qingdao, China, [8]Center for Ocean Mega-Science, Chinese Academy of Sciences, Qingdao, China

Key Points:
- The wind spectra, cospectra, and Ogive curve measured at a height of 8 m above the mean surface record swell-induced perturbations
- The influence of swell on the wind vector is analyzed based on the total stress as a vector sum of the turbulent stress and wave-induced stress
- The magnitude and angle of the wind stress changed by swell waves depend on the relative angle between the turbulent stress and swell direction

Correspondence to:
J. Song and J. Huang,
songjb@zju.edu.cn;
hj@grmc.gov.cn

Citation:
Zou, Z., Song, J., Li, P., Huang, J., Zhang, J. A., Wan, Z., & Li, S. (2019). Effects of swell waves on atmospheric boundary layer turbulence: A low wind field study. *Journal of Geophysical Research: Oceans*, *124*, 5671–5685. https://doi.org/10.1029/2019JC015153

Received 19 MAR 2019
Accepted 17 JUL 2019
Accepted article online 24 JUL 2019
Published online 13 AUG 2019

Abstract The effect of swell waves on atmospheric boundary layer turbulence under low winds was explored using data from a fixed platform located in the South China Sea. The wind spectra, cospectra, and Ogive curve measured at a height of 8 m above the mean sea surface provided direct evidence that wind stress was affected by swell waves. To interpret such phenomena, an improved approach was derived based on the fact that the total wind stress was the vector sum of turbulent stress and wave-coherent stress. Different from the approaches of earlier studies, our approach did not align the turbulent stress with the mean wind speed. The influence of swell waves on the magnitude and direction of the total wind stress was analyzed using our approach. The results showed that the wave-coherent stress derived from our data accounted for 32% of the total wind stress. The magnitude and angle of the wind stress changed by swell waves depended on the relative angle between the turbulent stress and swell direction.

Plain Language Summary A better understanding of the interactions between ocean waves and the atmospheric boundary layer (ABL) is crucial for predicting the future state of air-sea interactions and the long-term development of the climate. Many recent studies have shown that the behavior of the ABL under swell waves (ocean waves with old ages) is significantly different from that under young waves. In this study, we focus on the effect of swell waves on ABL turbulence by using observational data from a fixed platform located in the South China Sea. We show that swell waves can not only induce upward momentum but also absorb momentum. The change in the wind stress vector by swell waves also depends on the relative angle between the turbulent stress and swell direction. To interpret these phenomena, an improved approach is given here based on the fact that the total wind stress is the vector sum of turbulent stress and wave-coherent stress.

1. Introduction

Several decades of studies (Andreas et al., 2012; Drennan et al., 2003; Edson et al., 2013; Fairall et al., 2003; Guan & Xie, 2004; Liu et al., 2012; Mahrt et al., 2018; Smith, 1980; Smith et al., 1992; Vickers et al., 2015; Wu, 1980) have focused on the parameterization of wind stress over the oceans. These studies demonstrated a clear increasing trend of the drag coefficient with wind speed under a moderate wind range. However, wind speeds below 5–7 m/s or above 20–25 m/s are less understood: the former always encounters swell waves (e.g., Hanley et al., 2010), and the latter is easily influenced by sea spray (e.g., Holthuijsen et al., 2012; Takagaki et al., 2012). In this study, we focus on the former, that is, the interaction between swell waves and wind stress under light wind speeds.

With increasingly available observational data from open sea, aircraft or fixed platforms, studies (e.g., Fairall et al., 2006; García-Nava et al., 2009; Grachev et al., 2011; Vickers et al., 2013; Zou et al., 2017) have shown that the drag coefficient, which is usually written as a function of mean wind speed, becomes dramatically scattered under light wind speeds, resulting in many uncertainties for improving the accuracy of atmospheric and oceanic models. Babanin and Makin (2008) summarized a series of physical

properties and phenomena, including wind speed, wave age and slope, and the gustiness of wind, and suggested that the drag coefficient should incorporate all these factors into the final parameterization to reduce scatter.

Among the above factors, swell waves, which travel faster than local winds and have long wave lengths and old wave ages, have attracted the attention of researchers for a long time. For example, Rieder and Smith (1998) showed that swell waves have a significant effect on both the magnitude and direction of wind stress. By removing the swell effect from wind stress, Rieder and Smith found the behavior of residual stress such as stress under wind sea. The studies of Grachev and Fairall (2001) and Grachev et al. (2003) showed that fast-traveling swell waves can diminish the wind stress and drive the stress vector to deviate from the wind direction. The shift in the wind vector away from the wind direction was also reported by Zhang et al. (2009). García-Nava et al. (2012) showed that the presence of swell waves can reduce the wind stress by modifying the sea roughness. Data from the Baltic Sea Swell Experiment also show that the drag coefficient is systematically lower than Rough Evaporation Duct experiment (Högström et al., 2013; Högström et al., 2015). In addition, the experiment of Kahma et al. (2016) gives a direct evidence to demonstrate that an upward momentum can be generated by swell waves.

The scatter of the drag coefficient is a result of swell waves affecting atmospheric turbulence. To describe the turbulent process occurring in the atmospheric boundary layer (ABL), atmospheric and oceanic models typically adopt the Monin-Obukhov similarity theory (MOST; Monin & Yaglom, 1971) to allow momentum transfer from the air to water. The MOST is also widely used to convert meteorological data among different heights and atmospheric stabilities, and its logarithmic layer assumption is the basic theory to compute wind stress using wind profiles. Under swell conditions, however, field measurements (Högström et al., 2009; Högström et al., 2013; Smedman et al., 2009) show that swell waves can exert a singular point in the wind profile, which cannot be modeled within the framework of the traditional MOST. The invalid MOST was further confirmed by direct numerical simulation (Kihara et al., 2007; Sullivan et al., 2000), large-eddy simulation (Jiang et al., 2016; Nilsson et al., 2012; Sullivan et al., 2008 and Sullivan et al., 2014), and simplified theoretical models (Hanley & Belcher, 2008; Semedo et al., 2009; Song et al., 2015 and Zou et al., 2018).

The inertial dissipation method (IDM) is also influenced by swell waves. Based on the MOST and turbulent kinetic energy budget, the high-frequency portion of the inertial subrange is applied by IDM to determine the wind stress. Studies (Pan et al., 2005; Sjöblom & Smedman, 2004) have shown that under swell conditions, the IDM is not consistent with the eddy correlation method. It has also been shown that the transport terms in the turbulent kinetic energy budget should not be treated as wind seas (Högström et al., 2009).

The effect of swell waves on ABL turbulence is a complex process, and more direct observations are required to study the effects of swell waves on drag coefficients or the MOST. However, apart from a few studies (Högström et al., 2015; Högström et al., 2018) showing a swell-related turbulent regime in cospectra (defined in section 2), direct evidence of wind stress affected by swell waves from the turbulent level is still rare, especially when swell waves propagate in directions different from the wind direction. Thus, instead of studying the effect of swell waves on drag coefficients or the MOST, this study focuses on direct evidence that wind stress is affected by swell waves by analyzing cospectra and Ogive curves (cumulative summation of cospectra). Then, effect of swell waves on wind stress and vectors is analyzed when the directions of swell waves and the wind are different.

This paper is organized as follows. Section 2 gives the methods used in this study; section 3 introduces the measurements; section 4 shows the results, including direct evidence of the effect of swell waves on cospectra and Ogive curves, a physical interpretation, and the behavior of wind stress and vectors under swell conditions; and finally, a discussion and conclusion are presented.

2. Methods

Turbulent flow in the ABL can be treated as a superposition of different sized eddies. These eddies derive energy from background flow and interactions with themselves, thus yielding increasingly smaller-scale eddies until the eddies are small enough to convert their energy to heat. When wind blows over the

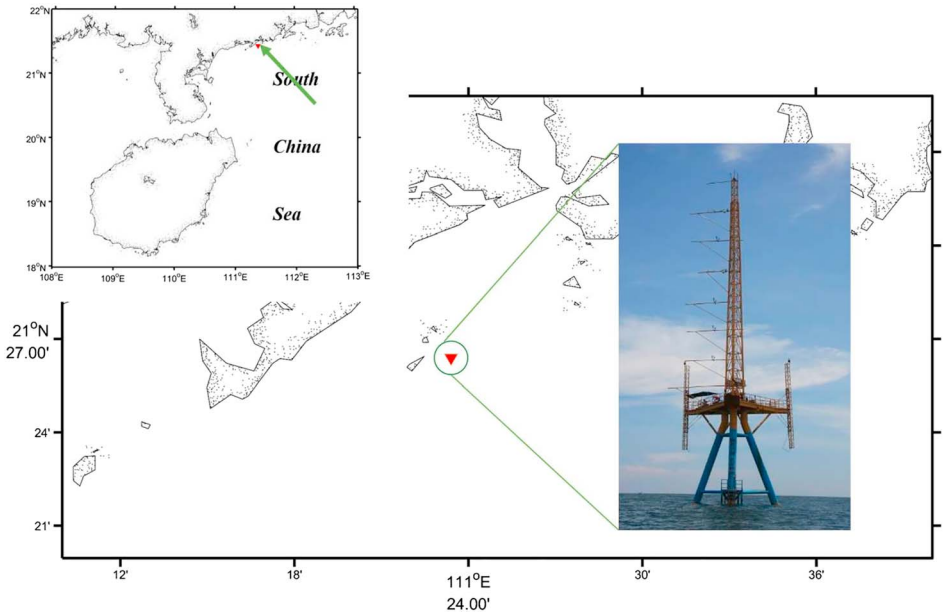

Figure 1. The location and the structure of the platform

water surface, the surface waves generated by the wind exert wave-coherent perturbations on the wind (Harris, 1966) due to the difference in the pressure distribution before and after wave crests (e.g., Buckley & Veron, 2016). The wave-coherent perturbations merge into turbulence, significantly changing the stress and vectors when the stress is computed by the eddy correlation method (Rieder & Smith, 1998) and invalidating the MOST within the wave boundary layer (Babanin et al., 2018).

To better understand the effect of swell waves on ABL turbulence, it is key to determine the wave-coherent stress, which is a vital part of the total wind stress (Hristov & Ruiz-Plancarte, 2014):

$$\boldsymbol{\tau} = \boldsymbol{\tau}_{vis} + \boldsymbol{\tau}_{turb} + \boldsymbol{\tau}_{wave}, \tag{1}$$

where $\boldsymbol{\tau}_{vis}$ is the viscous stress and can be omitted because it is only important in the near-surface viscous sublayer. $\boldsymbol{\tau}_{turb}$ is the turbulent stress only generated by the gradient of the mean wind U, as well as buoyancy. Usually, it is positive because the wind speed decreases with decreasing height. $\boldsymbol{\tau}_{wave}$ is the wave-coherent stress. Waves with low phase speeds relative to the wind speed absorb the momentum, while faster-traveling waves exert upward momentum. The interactions between wind and waves also depend on their angles: if waves and wind travel in opposite directions, waves are also sinks of momentum (Grachev & Fairall, 2001). The wave-coherent stress is assumed to decay exponentially with height. Recent measurements and numerical studies (Högström et al., 2009; Semedo et al., 2009) have shown that the layer where the wave-coherent stress is significantly influenced is typically only one- or two-wave height for wind sea, but the swell can penetrate all the atmospheric boundary.

If the waves travel in a direction different from the wind, the stresses should be considered as vectors:

$$\begin{aligned} \boldsymbol{\tau} &= -\rho\langle uw\rangle\,\mathbf{i} - \rho\langle vw\rangle\,\mathbf{j}\ , \\ \boldsymbol{\tau}_{turb} &= -\rho\langle u'w'\rangle\mathbf{i} - \rho\langle v'w'\rangle\,\mathbf{j}\ , \\ \boldsymbol{\tau}_{wave} &= -\rho\langle \widetilde{u}\widetilde{w}\rangle\mathbf{i} - \rho\langle \widetilde{v}\widetilde{w}\rangle\mathbf{j}\ , \end{aligned} \tag{2}$$

here, ρ is the air density; $\mathbf{i}$ and $\mathbf{j}$ represent the longitudinal (x axis) and lateral (y axis) unit vectors, and the x axis is aligned with the wind direction; $<\bullet>$ is the time averaging operator; and u, v, and w represent the wind fluctuation after removing the mean wind speed, which can be further decomposed into wave-coherent perturbations ($\widetilde{u}, \widetilde{v}, \widetilde{w}$) and turbulence ($u'$,$v'$,$w'$) based on triple decomposition (Buckley & Veron, 2016).

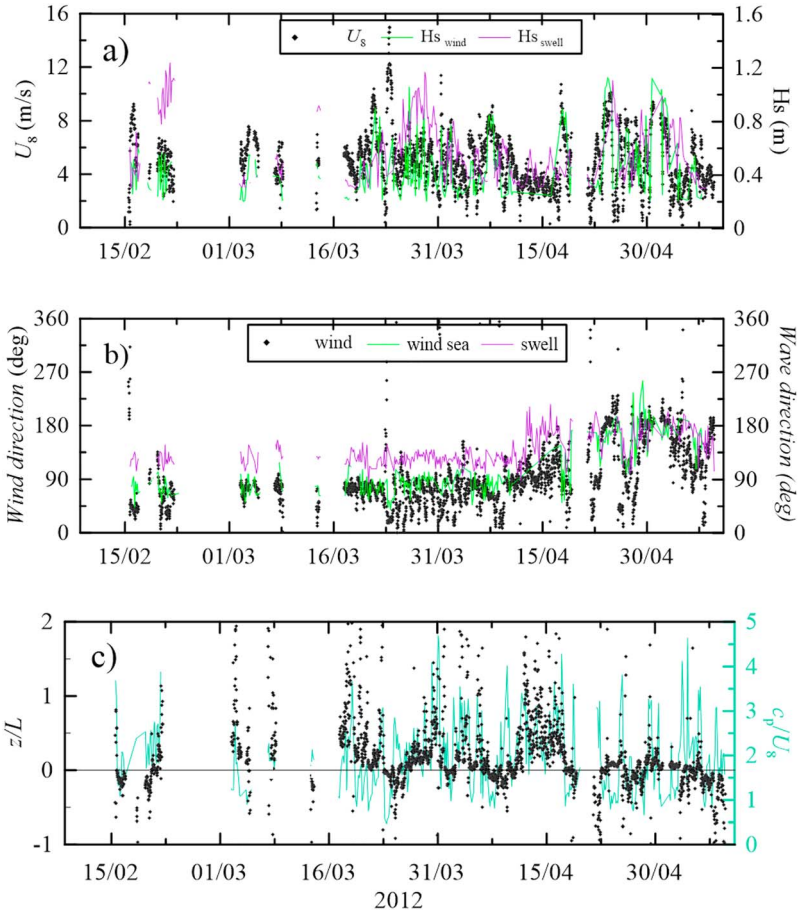

Figure 2. Time series of (a) wind speed and significant wave height, (b) wind direction and wave direction, and (c) atmospheric stability and wave age during observation. The horizontal ordinate shows the local time. The dominant peak wave speed is used to compute the wave age.

From a turbulent level, the spectra form of stress in equation (2) can also be expressed as (Grachev & Fairall, 2001)

$$\begin{aligned}\boldsymbol{\tau} &= -\int_0^{+\infty}\rho Co_{uw}(f)df\,\mathbf{i} - \int_0^{+\infty}\rho Co_{vw}(f)df\,\mathbf{j},\\ \boldsymbol{\tau}_{turb} &= -\int_0^{+\infty}\rho Co_{u'w'}(f)df\,\mathbf{i} - \int_0^{+\infty}\rho Co_{v'w'}(f)df\,\mathbf{j},\\ \boldsymbol{\tau}_{wave} &= -\int_0^{+\infty}\rho Co_{\tilde{u}\tilde{w}}(f)df\,\mathbf{i} - \int_0^{+\infty}\rho Co_{\tilde{v}\tilde{w}}(f)df\,\mathbf{j},\end{aligned} \tag{3}$$

where Co is the cospectra, and f is the frequency in Hz. The negative Co in the x axis represents the downward transport of momentum (from air to water), and vice versa. The negative (positive) Co in the y axis represents the wind stress directed to the left (right) on the wind vector.

Based on the cospectra, the Ogive curve is defined as the integral of cospectra from the highest frequency to the frequency of interest:

$$\mathbf{O_g}(f) = Og_x\,\mathbf{i} + Og_y\,\mathbf{j} = \int_{f_{\max}}^{f} Co_{uw}(f)df\,\mathbf{i} + \int_{f_{\max}}^{f} Co_{vw}(f)df\,\mathbf{j}, \tag{4}$$

where $\mathbf{O_g}$ is the Ogive curve. The Ogive curve contains both a turbulent effect and a swell effect because Co_{uw} and Co_{vw} are used in equation (4).

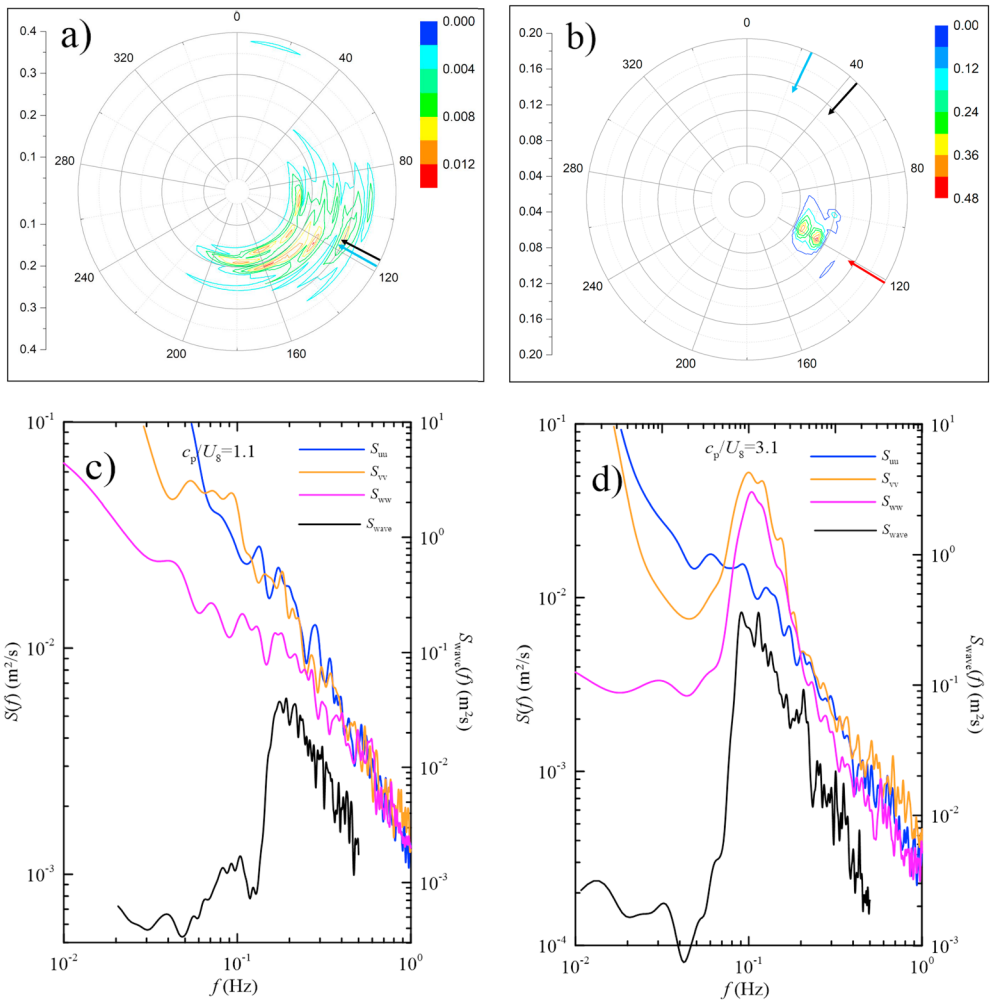

Figure 3. Directional wave spectra and frequency spectra of the wind speed fluctuations at a height of (a and c) 8 m at 17 o'clock on 5 May and (b and d) 3 o'clock on 29 March. Panels (a) and (b) directional wave spectra under wind sea and swell conditions, respectively; the black, green, and red arrows are the wind direction, total stress direction, and swell wave direction, respectively. Panels (c) and (d) correspond to the three-dimensional wind spectra for wind sea and swell wave conditions. The blue line (S_{uu}), orange line (S_{vv}), and magenta line (S_{ww}) represent the spectra of longitudinal, lateral, and vertical wind fluctuations, respectively. The black lines (S_{wave}) are wave spectra computed from integrating directional wave spectra.

Additionally, we define the stress angles based on equation (2):

$$\begin{aligned} \alpha &= \arctan\left(\tau_y/\tau_x\right) \ , \\ \alpha_{turb} &= \arctan\left(\tau_{turb\ y}/\tau_{turb\ x}\right) \ , \\ \alpha_{wave} &= \arctan\left(\tau_{wave\ y}/\tau_{wave\ x}\right) \ , \end{aligned} \tag{5}$$

where α, α_{turb}, and α_{wave} represent the angles of total stress, turbulent stress, and wave stress that deviated from the wind direction, respectively. The positive angles correspond to the stress vector oriented to the left of the wind vector.

According to the definition of equations (3) and (5), the turbulent stress can both point to the left (corresponding to $Co_{v'w'}<0$) and right ($Co_{v'w'}>0$) side of wind vector, combining with the negative or positive wave-coherent stress ($\pm Co_{\tilde{u}\tilde{w}}$,$\pm Co_{\tilde{v}\tilde{w}}$), the effect of swell waves on wind stress can be separated into eight cases. These cases will be analyzed using cospectra and Ogive curve.

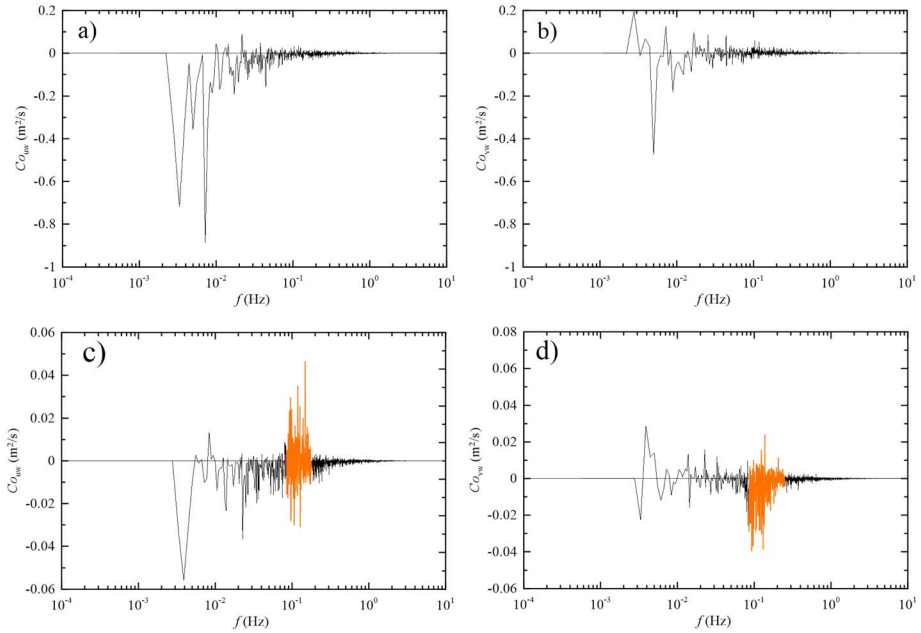

Figure 4. Along-wind and across-wind cospectra as a function of frequency using the data shown in Figure 3. (a and b) The wind sea case at 17 o'clock on 5 May. (c and d) The swell case at 3 o'clock on 29 March. The orange color in the figure represents the wave-influenced region.

3. Measurements

The measurements used in this study were taken at a fixed platform located in the South China Sea. Figure 1 shows the location and the structure of the platform. The body of the platform is a hollow steel structure anchored by three huge concrete tanks on the seafloor. The nearest distance between the platform and coastline is approximately 6.5 km, and the water depth at the platform location is approximately 16 m.

During the measurements, several eddy-correlation systems, including ultrasonic anemometer, CO_2/H_2O analyzer, infrared radiometer and temperature and relative humidity measurement systems, were mounted at 8, 20, 28, and 36 m above the mean sea level to record the temperature and three wind components. Five low-frequency marine wind monitors were mounted at 31.3, 23.4, 20.0, 16.4, and 13.4 m to measure wind speed and direction. An acoustic wave and current (AWAC) sensor (Nortek, Rud, Norway) on the seabed was used to measure directional wave data.

In this study, turbulence and waves measured from 6 February to 8 May 2012 were used. The turbulence observed by the high-frequency ultrasonic anemometer (Gill R3-50) mounted at a height of 8 m was selected. The turbulence was observed at a frequency of 20 Hz, and the instruments pointed to the east. Waves were observed by the AWAC every three hours, and each wave measurement lasted 2048 s with a sampling frequency of 1 Hz. To guarantee the accuracy of the results, strict quality control procedures, including spike removal, tilt correction, and mesoscale motion removal (Zou et al., 2017), were used before analyzing the effect of swell waves on ABL turbulence.

Figure 2 shows the observational time series for several key variables. The high-frequency wind observations taken at a height of 8 m were averaged every 30 min to obtain the mean wind speed U_8, and the residual was used to compute the spectra, cospectra, and Ogive curves in the next section. During this period, the winds were not strong, mostly ranging from 1 to 6 m/s; the marine surface waves were almost completely dominated by swell, with a significant swell wave height Hs_{swell} ranging from 0.4 to 1.2 m, while the wind following the significant wind wave height Hs_{wind} mainly concentrated in a range of 0.3–0.8 m. The wind directions were predominantly from the Northeast before April but slowly changed to the southeast at the end of the measurement period. Unlike the winds, the swell wave directions were nearly constantly toward the northwest, giving a relative angle between the wind and swell waves ranging from -120 to 50°. Note that in this paper, all directions for the winds and waves were calculated using meteorological convention ("from").

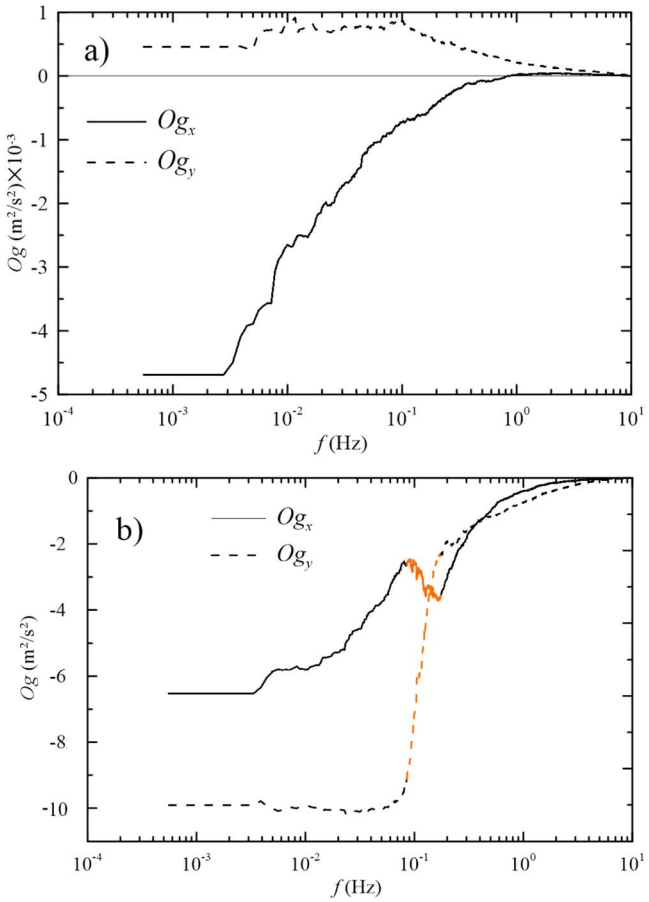

Figure 5. Ogive curves computed using data in Figure 3. (a) Wind sea (17 o'clock on 5 May) and (b) swell (3 o'clock on 29 March) cases. The solid lines represent the longitudinal Ogive curves, and the dashed lines represent the lateral Ogive curves.

The atmospheric stability and wave age (defined as c_p/U_8, where c_p is the dominant peak wave speed) data are shown in Figure 2c. It can be seen that the ABL encountered both stable and unstable conditions, with mostly -1<z/L<1, where z is height above sea surface and L is Obukhov length scale. For wave age, we used wind speeds measured at a height of 8 m above the sea surface rather than U_{10} to determine the wave ages because the MOST is invalid under swell conditions. It can be seen that swell waves ($c_p/U_8 > 1.2$) generally dominated the observations. To analyze the mechanism by which swell waves influence ABL turbulence, only wind spectra with a pronounced peak at the dominant wave frequency (see Figure 3) were selected.

4. Results

4.1. Direct Evidence of the Effect of Swell Waves on Wind Stress

Figure 3 shows the directional wave spectra and corresponding power spectra for the three wind speed components. Two examples were selected to address the difference in wind spectra under wind sea and swell wave: one example (Figures 3a and 3c) was under wind sea conditions, and the other example (Figures 3b and 3d) was under swell conditions. It is evident that the behavior of the wind spectra under the swell case (Figure 3d) is much different from that under the wind sea case (Figure 3c), with a distinct peak in the spectra centered at the frequency of the dominant wave. This feature has been widely reported in earlier studies, such as Rieder and Smith (1998), Soloviev and Kudryavtsev (2010), and Högström et al. (2015).

Figures 4 and 5 show the cospectra and Ogive curves using the same data as Figure 3. For wind waves, the along-wind cospectra are below zero, with some randomly positive points, indicating the downward transport of momentum over all frequencies. The magnitude of Co_{uw} increases with decreasing frequency, and the low-frequency parts ($f < -0.05$ Hz) contribute mostly to the total wind stress. The Ogive curve contains the same information as the cospectra. It decreases monotonously with decreasing frequency (Og_x in Figure 5a). Figure 4b shows that the lateral cospectra seemed to spread randomly over the zero line; however, the integral of Co_{vw} is nonzero (Og_y in Figure 5a), suggesting that the stress points to the right side of the wind vector (Figure 3a).

Both the cospectra and Ogive curve under swell conditions show significant differences from those under wind waves. Figures 4c and 4d show a special region (orange color) that appeared in the dominated wave frequency; this region has both positive and negative segments. The positive segment in Co_{uw} causes an abrupt increase with decreasing frequency in Og_x, while Og_y suddenly decreases in this region due to the negative segment of Co_{vw} (Figure 5b); thus, the total stress deviates greatly from the wind vector. Compared with the wind case, we infer that the anomaly in the cospectra and Ogive curve is related to the swell waves. The swell-related region in the cospectra is consistent with Högström et al. (2018), who also give a positive region in the cospectra for wind speeds less than 4.5 m/s; however, different from the results of Högström et al. (2015) and Högström et al. (2015, 2018) for wind speeds greater than 4.5 m/s, the cospectra have pronounced negative peaks only at the dominant swell frequency. The reason why the cospectra have both positive and negative regions will be interpreted in section 4.2.

The examples in Figures 4c and 4d and 5b indicate that the influence of swell on wind stress is apparent and that the abrupt change in the Ogive curve can be considered a distinct feature indicating the influence of swell waves on wind stress. These examples correspond to a case in which the wind follows a swell wave, but the turbulent stress points to the left side of the wind vector. By considering all data, the schematics of other cases, together with the case in Figure 5, are shown in Figure 6. All cases have a negative $Co_{u'w'}$. Cases 1, 3, and 5 have a negative $Co_{v'w'}$, but cases 2, 4, and 6 have a positive $Co_{v'w'}$; the longitudinal wave-

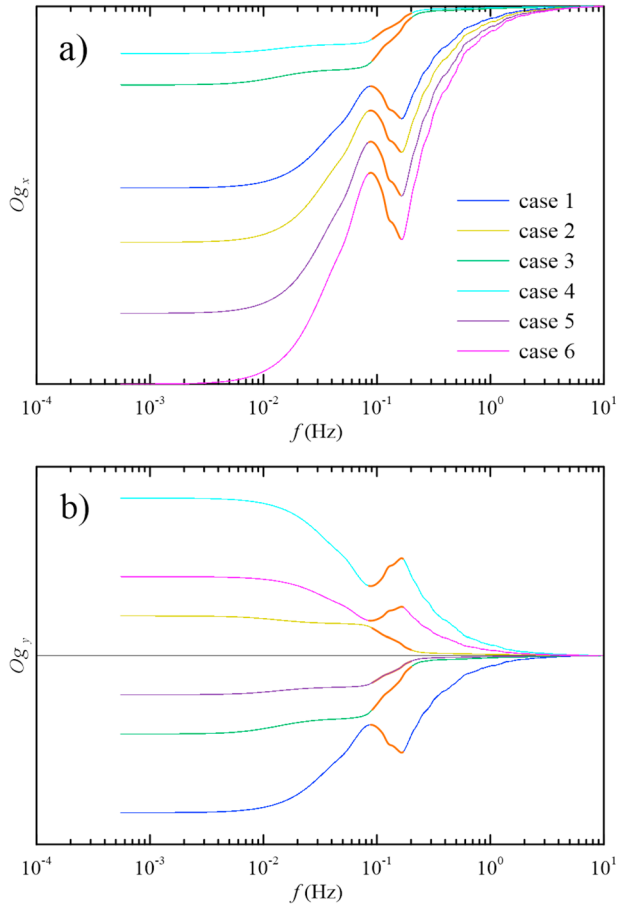

Figure 6. Schematic of along-wind and across-wind Ogive curves influenced by swell waves. The orange color represents the wave-influenced region. (a) longitudinal Ogive curve and (b) lateral Ogive curve.

coherent cospectra in cases 1, 2, 5, and 6 are positive, and the lateral wave-coherent cospectra are positive in cases 1 and 2 and negative in the other cases. These features will be analyzed in the next section. It should be noted that there are still two cases not shown in our data due to the influence of platform structure.

4.2. Physical Interpretation

The total wind stress is the integral of the cospectra over all frequencies, thus containing both turbulent stress and wave-coherent stress. The difference between turbulent stress and wave-coherent stress within the wave boundary layer is that wave-coherent stress is contained in a narrow frequency range corresponding to the peak in the wave spectra, while turbulent stress comes from a wider range of frequencies (approximately 10^{-3} to 10 Hz in this study). Based on this concept, we analyzed the behavior of the Ogive curves shown in Figure 6. As mentioned above, the wind wave-coherent stress decays more rapidly than the swell; hereafter, only the swell part of τ_{wave} will be considered in this study.

The basic theory of the effect of swell waves on wind vectors has been explored by Grachev et al. (2003). In their study, the turbulent stress was assumed to be aligned in the same direction as wind, that is, the turbulent stress. $\alpha_{turb} = 0°$. However, the turbulent stress direction is actually controlled by a shear vector other than the wind direction. Ekman theory predicts that the wind vector rotates clockwise with height in the Northern Hemisphere, driving the turbulent stress vector to deviate from the wind direction (Mahrt et al., 2001), and the Coriolis force in the boundary layer can be enlarged when the wave-coherent stress appears (Hanley & Belcher, 2008). In addition, the deviation of turbulent stress from the wind is also influenced by buoyancy; for example, Mahrt et al. (2001) reported an angle of approximately 25° between two vectors under very unstable conditions using the Microfronts data collected in Kansa; Geernaert (1988) showed the turbulent stress vector was to the left of the flow during stable stratifications (this vector points to right of the flow based on the definition of equation (5) in this study), while for unstable stratifications, turbulent stress vector was to the right. It should be noted that the deviation in wind stress from the wind vector always appears, even under wind sea conditions or above rigid land surfaces. Thus, in this study, the relative angle between the turbulent stress and wind direction was not set to zero.

Figure 7 shows a schematic of the effect of swell-coherent stress on turbulent stress. Here, the wind vector was set to point toward the east, and the angle between the turbulent stress vector and wind direction was acute.

Figures 7a and 7c show cases in which winds follow swell waves, where swell exerts an upward transfer of momentum from the ocean to atmosphere. At this time, the longitudinal cospectra are negative and, together with the upward momentum, cause an abrupt increase in the Ogive curve at the dominant swell wave frequency (cases 1, 2, 5, and 6 in Figure 6a). However, the cross-wind stress is not simple because swell waves can generate both downward and upward momentum in vertical coordinates. For upward momentum, the behavior of the Ogive curve, as in cases 1 and 2 in Figure 6b and cases 5 and 6 in Figure 6b, corresponds to downward momentum.

In the cases in which the wind blows against the swell waves (Figures 7b and 7d), swell will drag the wind and absorb energy, thus making the along-wind stress larger than the along-wind turbulent stress, inducing a sharp decrease in the Ogive curve (cases 3 and 4 in Figure 6a). The behavior of cross-wind stress in Figures 7b and 7d is similar to that in Figures 7a and 7c. It should be noted that the cases in Figure 7d did not appear in our data due to the structural effect of the platform; hence, no wind blew from 240 to 340°.

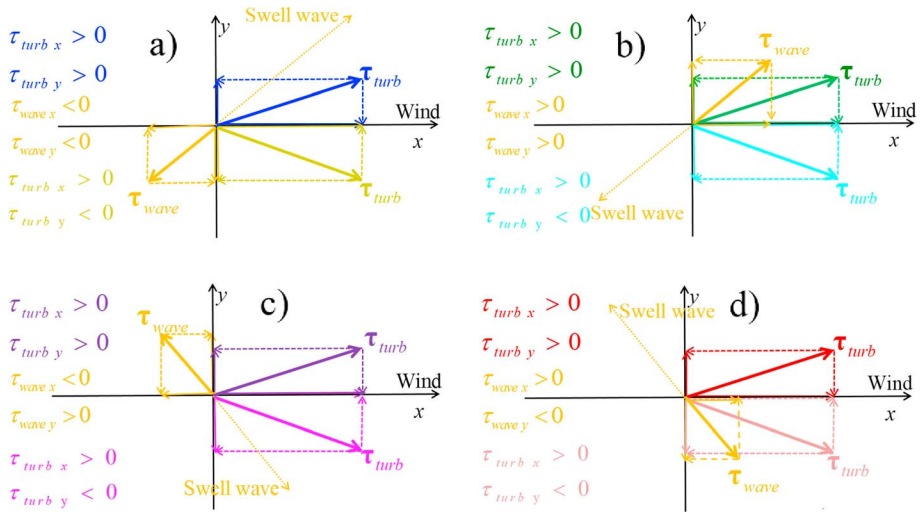

Figure 7. Schematic of the effect of swell-coherent stress on turbulent stress.

The above analysis shows that the swell exerts an upward momentum along the wind direction when the wind blows over the swell. This momentum is confined to a narrow band at frequencies of dominant swell waves, thus leading to a positive region in Figure 4c. When wind blows against swell, the swell wave-coherent stress has the same sign as the turbulent stress, and the two stresses mix together to cause a negative peak in the cospectra.

4.3. Wind Stress and Vectors

To better understand the effect of swell on turbulent stress, swell wave-coherent perturbations should be extracted first. Recently, Wu et al. (2018) showed that the wave-coherent stress derived from the orthogonal projection of wind onto Hilbert space (Hristov et al., 2003) and the linear transformation method (Grare et al., 2013) are consistent with each other. However, these methods are not valid in our measurements because the frequency of AWAC is less than that of turbulence. By splitting the wind stress into low, middle, and high frequencies, Rieder and Smith (1998) showed that the middle frequencies correspond to the frequencies of dominant swell waves and that the stress of this category is tied to the direction of the swell waves. Högström et al. (2015) and Högström et al. (2018) also showed that the stress in the middle category is a function of swell-significant wave height. Their middle category corresponds to the swell-related region shown in Figures 4c and 4d.

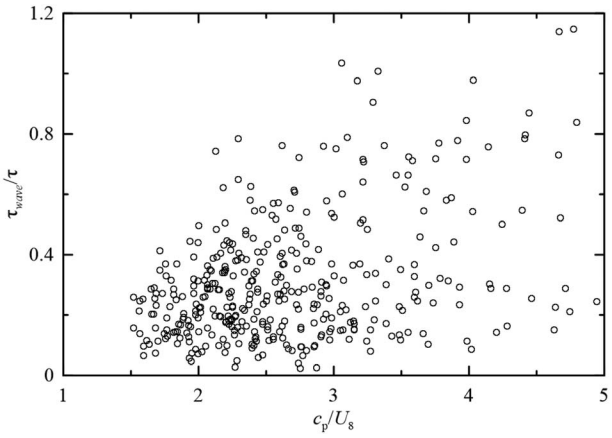

Figure 8. Changes in the ratio of wave-coherent stress to total wind stress with wave age

In this study, the swell-related region (the orange region in Figures 4c and 4d) was first defined by identifying the swell-related peaks in the wind spectra; then, the swell-coherent stress was computed using the following method. For cases 1, 2, 5, and 6, the positive segment of the swell-related region along the wind cospectra corresponded to the upward momentum exerted by swell waves; thus, the $\tau_{wave\ x}$ can be computed by $\tau_{wave\ x} = -\rho \int_{f_{down}}^{f_{up}} Co_{wu}(f)df$ where $Co_{wu}(f)>0$, and the f_{down} and f_{up} represent the down and up limit frequency of positive segment in the swell-related region, and $\tau_{wave\ y}$ was computed by $\tau_{wave\ x}\tan(\alpha_{wave})$. For case 4, $\tau_{wave\ y}$ was computed by the integral of the negative segment of the swell-related region across the wind cospectra, and $\tau_{wave\ x}$ was computed by $\tau_{wave\ y}/\tan(\alpha_{wave})$. For case 3, it was difficult to distinguish τ_{wave} from τ_{turb} in both the along- and across-wind cospectra; here, their sum was simply considered wave-coherent stress.

Figure 8 shows the fraction of the swell-coherent stress against c_p/U_8. The figure shows that the swell-coherent stress is approximately 5–50% of the

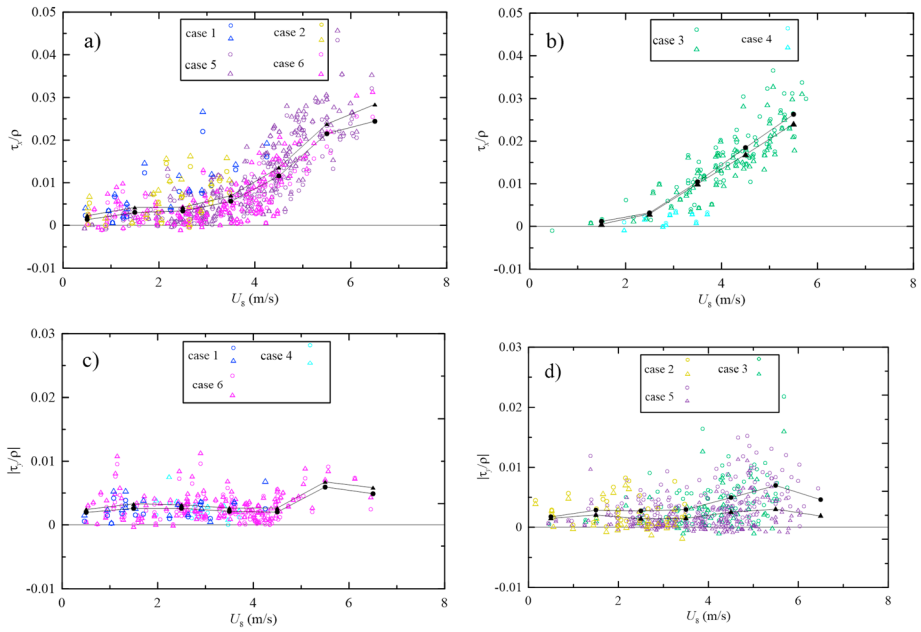

Figure 9. Changes in (a and b) along-wind and (c and d) across-wind stress components with wind speed. The circles and triangles represent the total stress and turbulent stress, respectively. The black color shows the mean values, and the other colors correspond to the cases in Figures 6 and 7.

total stress. In some cases, especially under extremely large wave ages, the swell-coherent stress can exceed 80% of the total stress. In general, the fraction of the swell-coherent stress increases with wave age, giving an average of 32%, a bit larger than the results of Wu et al. (2018) derived from data collected at a height of 9.9 m above the sea.

By removing the swell stress from the total stress, the turbulent stress is given in Figure 9; the total wind stress is also included in this figure for comparison. To discern the difference between the turbulent stress and total wind stress, we separated the along-wind data onto two figures: Figure 9a corresponds with the wind blowing over swell waves, and Figure 9b corresponds with the wind blowing against the swell waves. The across-wind data were also separated based on whether the magnitude of the across-wind stress was enlarged by swell or not.

The total stress in Figure 9 shows that the along-wind stress increases monotonically with increasing wind speed. However, on average, case 3 has a higher value than the cases in Figure 9a. We noted that case 3's wind is mostly blowing from the coastal region, while the other cases have longer fetches. The younger and steeper waves in the limited fetch coherently have a larger drag coefficient, leading to the higher values of case 3. This has been reported by Zou et al. (2017) for the same platform. Unlike the along-wind stress, the across-wind stress does not have a clear tendency to increase with wind speed but appears to randomly overlap with the zero line, especially for $U_8 < 4$ m/s, which is consistent with Grachev et al. (2003).

Compared with mean turbulent stress (black triangles) and total stress (black circles), swell waves have a remarkable effect, with an increase in along-wind stress for cases 1, 2, 5, and 6, and a decrease in along-wind stress for cases 3 and 4. The magnitude of the across-wind stress also increases for cases 1, 4, and 6 and decreases for cases 2, 3 and 5.

Counter- and across-swell are usually considered to result in wind stresses larger than pure wind sea, but the following swell can decrease wind stress (e.g., Donelan et al., 1997; Grachev & Fairall, 2001; Högström et al., 2013). However, Figure 9 shows that when $\alpha_{turb} \neq 0°$, the magnitude of the total wind stress should be expressed as

$$|\boldsymbol{\tau}| = \sqrt{|\boldsymbol{\tau}_{turb}|^2 + |\boldsymbol{\tau}_{wave}|^2 + 2|\boldsymbol{\tau}_{turb}||\boldsymbol{\tau}_{wave}|\cos(\alpha_{turb} - \alpha_{wave})}, \quad (6)$$

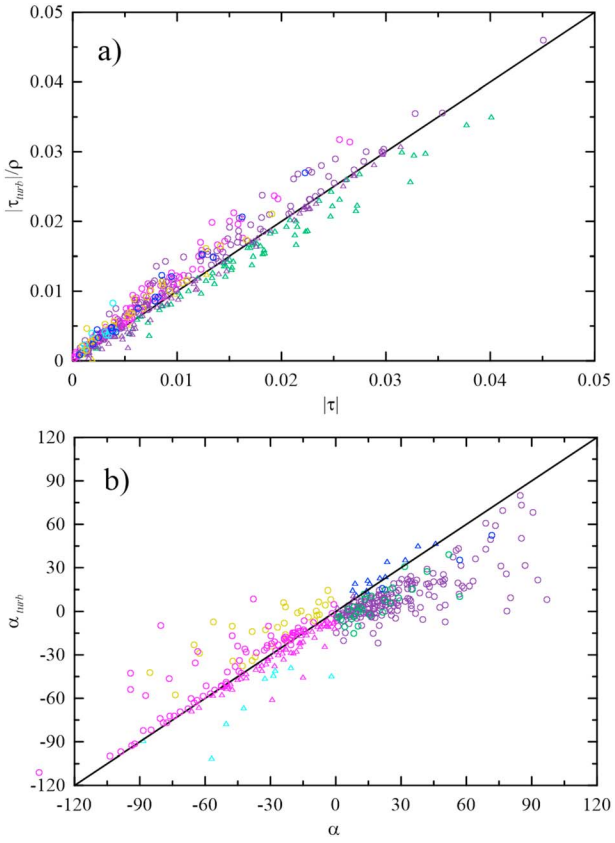

Figure 10. (a) Comparison between the magnitude of the total wind stress and turbulent stress and (b) stress angle compared with the turbulent stress angle. The colors are consistent with the cases in Figures 6 and 7. The circles and triangles in (a) correspond with cos ($\alpha_{turb} - \alpha_{wave}$) values less than and larger than -0.5|τ_{wave}/τ_{turb}|, and in (b), the circles and triangles correspond with turbulent stress that deviates from and approaches the wind vector, respectively.

According to equation (6), swell exerts upward momentum when cos ($\alpha_{turb} - \alpha_{wave}$) < -0.5|$\tau_{wave}$|/|$\tau_{turb}$|to make the total wind stress less than the turbulent stress; for cos ($\alpha_{turb} - \alpha_{wave}$) > -0.5|$\tau_{wave}$|/|$\tau_{turb}$|, the total stress becomes larger than the turbulent stress; and for cos ($\alpha_{turb} - \alpha_{wave}$) = 0.5|$\tau_{wave}$|/|$\tau_{turb}$|, swell does not contribute to wind stress. A comparison between the magnitudes of the total wind stress and turbulent stress is shown in Figure 10a.

The change in the total stress angle by swell waves can be computed by vector synthesis: if the swell wave direction α_{wave} ranges from 0° to α_{turb} or if the stress fulfills |τ_{wave}sin (α_{wave})|≤|τ_{wave}sin (α_{turb})|& sin (α_{wave})×sin (α_{turb})<0, the stress vector approaches the wind vector; when α_{wave} = α_{turb} or α_{turb}+180°, the stress vector remains in its direction, and the other stress vectors deviate from the wind vector. This feature is much different from the results of earlier studies (e.g., Chen et al., 2018), which attempted to remove the swell effect to reduce the deviated stress angle. The total stress angle compared with the turbulent stress angle is shown in Figure 10b.

5. Discussion

In this paper, the effect of swell waves on turbulent stress was studied. Unlike Grachev et al. (2003), who assumed that the turbulence stress is aligned with the wind vector, we assumed that there is an acute angle between the two vectors. This makes the interaction more complicated. Some studies suggest that buoyancy or the Coriolis effect has a significant effect on the turbulent stress direction; for example, Geernaert (1988) studied α_{turb} based on Navier-Stokes functions, although the model results were significantly smaller than observations. Figure 11 shows the change in the turbulent stress angle α_{turb} with atmospheric stability z/L. Although α_{turb} can be positive or negative for individual points, on average, turbulent stress points to the right of the wind under stable conditions and to the left of the wind under unstable conditions. This is consistent with the results of Geernaert (1988). Compared with the buoyancy effect, our data suggest that the influence of the Coriolis effect is small, generating an absolute value in the order of 1° under nearly neutral conditions.

Grachev et al. (2003) show that swell-coherent stress can also point to the swell direction in the cases of wind following swell waves. However, our measurements showed that the swell wave stress was always directed against the swell direction (Figures 7a and 7c). We note that these cases were usually associated with moderate to strong winds or weak swells. Furthermore, in these cases, the wave-coherent perturbations were small compared with the turbulence and could not exert a pronounced peak in spectra. As a result, the spectra were not easily distinguished from wind sea and thus were not selected in this study.

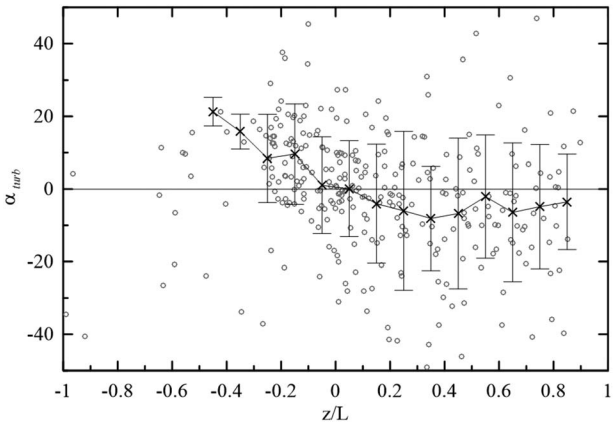

Figure 11. Distribution of the turbulent stress angle as a function of z/L.

Using the same platform but with data collected at a height of 17 m above the sea surface, Chen et al. (2018) showed that the effect of swell on the stress vector was quite small (their picture 6b), which seemed to conflict with our results (Figure 10b). Their vertical velocity spectra had a peak at the dominant wave frequency; thus, they argued that the wave boundary layer can extend to a height of 17 m. In our 20-m height spectra, the vertical velocity spectra are consistent with the results of Chen et al. (2018); however, the horizontal velocity spectra did not have significant swell- coherent perturbations. This may be because horizontal perturbations were induced by wave decay more quickly than vertical

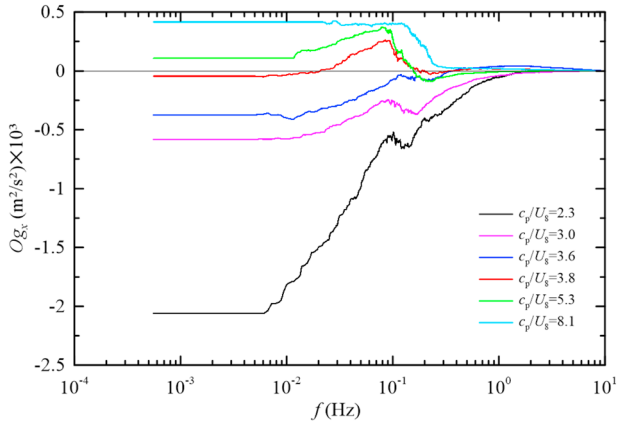

Figure 12. Examples of changes in along-wind Ogive curves with wave age. For wave ages equal to 5.3 and 8.1, we amplified the Ogive curves by a factor of 2 and 9, respectively, to avoid overlapping with the red line. From low to high wave age, the wind speeds are: 5.4, 4.2, 3.4, 3.2, 2.3, and 2.0 m/s.

perturbations (Wu et al., 2018); hence, the wave-coherent stress accounted for a small part of the total stress. In addition to the influence of height, Wu et al. (2017) also showed that buoyance has some effect on wave-coherent stress. As the convective boundary layer can suppress the wave-coherent turbulence, the effect of swell on the stress vector can be quite small.

Grachev and Fairall (2001) found that the momentum flux decreases monotonically with decreasing wind, reaching zero, and reversing at light wind speeds. Their cospectra showed both negative and positive segments at light wind speeds. Our results (Figure 4c) are consistent with the results of Grachev and Fairall. The positive region leads to an abrupt increase in the Ogive curves in Figure 6, indicating an upward momentum for wind following swell cases. As the wave age increases, the upward momentum tends to reduce the wind stress and finally leads to a sign reversal of the wind stress. Figure 12 gives some examples showing the evolution of the along-wind Ogive curve. It can be seen that the effect of wave stress increases with wave age; when the wave stress is sufficiently large, the total stress reverses sign; at this time, the wind profile decreases with increasing height (not shown here).

Many studies (e.g., Holthuijsen et al., 2012; Young, 2006) have shown that swell waves are also dominant under extreme winds, such as hurricanes. The interaction between swell waves and the ABL is critical in cyclone and hurricane predictions. However, our study focused on light wind speed conditions; thus, the behavior of the cospectra and Ogive curves may not be appropriate to describe the interactions between swell and the ABL under hurricane conditions. More data, especially direct observational turbulence data, are needed to address this issue.

In the end, we compared our data with earlier studies. For this purpose, the widely used COARE 3.0 (Fairall et al., 2003) algorithm was selected. Based on the Charnock parameter, the drag coefficient derived from COARE corresponds to the wind sea condition. Here, we check by removing swell-coherent stress whether the turbulent stress can represent the stress only generated by the wind sea. When comparing measurements under different heights and atmospheric stabilities, the MOST is a typical tool for transforming meteorological data into standard conditions, that is, a height of 10 m above the sea surface under neutral conditions. However, during swell conditions, the MOST is invalid. Thus, in the comparison, instead of converting our data to standard conditions, we input measured wind speed, atmospheric stability, and height data to COARE 3.0 to derive the pure wind sea drag coefficient. Figure 13 shows the comparison between our measurements and COARE 3.0. Here, only data from the open sea were selected to eliminate the possible effect of a limited fetch or inertial boundary layer. The results show that C_d computed by total wind stress was small compared with COARE for U_8 >2 m/s. Considering the swell effect, although the turbulent drag coefficient $C_{d\ turb}$ moved toward $C_{d\ COARE}$, $C_{d\ turb}$ was still less than $C_{d\ COARE}$, suggesting a nonlinear interaction between swell and ABL turbulence. This also indicates that it is not appropriate to compute wind stress by first computing the wind sea and then simply adding swell wave-coherent stress. To compute wind stress under swell conditions, new parameterization is needed.

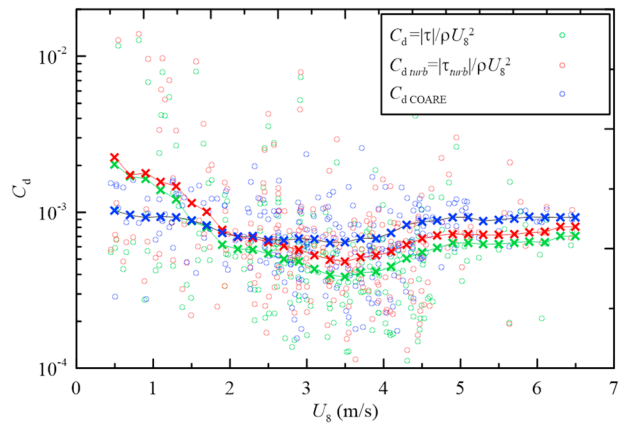

Figure 13. Comparison of the drag coefficient between our results and COARE. Here, C_d, $C_{d\ turb}$, and $C_{d\ COARE}$ were computed by total wind stress, turbulent stress and COARE 3.0, respectively. The cross marks denote bin-averaged values.

6. Conclusion

Using turbulence data from a fixed platform, this study analyzed the effects of swell waves, which were propagating in directions different from the wind, on ABL turbulence from turbulent level. The results showed that wind fluctuation spectra, cospectra and Ogive curves can provide a direct reflection of the effect of swell waves on ABL

turbulence, with a significant swell-related region in the dominant wave frequency. The positive region in the cospectra represents upward momentum, and it tends to decrease the along-wind stress or even make the stress reverse signs.

To interpret the effect of swell waves on ABL turbulence, we assumed that the total wind stress is the vector sum of turbulent stress and swell-coherent stress. Different from the approach of Grachev et al. (2003), our approach does not align the turbulent stress with the mean wind speed.

Based on our approach, the turbulent stress was derived after the swell-coherent stress was computed from the wind cospectra. The results show that the wave-coherent stress represents a large portion of the total wind stress, that is, an average of 32% of the total wind stress. The results also show that swell can reduce the along-wind stress of wind following swell cases but increase the along-wind stress of wind blowing against swell cases. The magnitude of across-wind stress also depends on the angle between the turbulent stress and wave-coherent stress. For total wind stress, only when $\cos(\alpha_{turb} - \alpha_{wave}) < -0.5|\tau_{wave}|/|\tau_{turb}|$ will swells make the total wind stress less than the turbulent stress. The stress vector approaches the wind vector when the swell wave direction ranges from 0° to α_{turb} or the stress fulfills $|\tau_{wave}\sin(\alpha_{wave})| \le |\tau_{turb}\sin(\alpha_{turb})|$ & $\sin(\alpha_{wave}) \times \sin(\alpha_{turb}) < 0$.

Acknowledgments
The data used in this study are available at https://www.seanoe.org/data/00506/61732/. We thank three anonymous reviewers for helping us improving our manuscript. We gratefully acknowledge the support of the National Natural Science Foundation of China (41806028, 41830533, and 41606024); the China Postdoctoral Science Foundation (2019 M65206), and the National Basic Research Program of China, Monitoring and Forecasting of Finescale Structure and Impact Assessment of Landfalling Typhoons (2015CB452800).

References

Andreas, E. L., Mahrt, L., & Vickers, D. (2012). A new drag relation for aerodynamically rough flow over the ocean. *Journal of the Atmospheric Sciences*, *69*(8), 2520–2537. https://doi.org/10.1175/jas-d-11-0312.1

Babanin, A. V., & Makin, V. K. (2008). Effects of wind trend and gustiness on the sea drag: Lake George study. *Journal of Geophysical Research*, *113*, C02015. https://doi.org/10.1029/2007JC004233

Babanin, A. V., McConochie, J., & Chalikov, D. (2018). Winds near the surface of waves: Observations and modeling. *Journal of Physical Oceanography*, *48*(5), 1079–1088. https://doi.org/10.1175/jpo-d-17-0009.1

Buckley, M. P., & Veron, F. (2016). Structure of the airflow above surface waves. *Journal of Physical Oceanography*, *46*(5), 1377–1397. https://doi.org/10.1175/jpo-d-15-0135.1

Chen, S., Qiao, F., Huang, C. J., & Zhao, B. (2018). Deviation of wind stress from wind direction under low wind conditions. *Journal of Geophysical Research: Oceans*, *123*, 9357–9368. https://doi.org/10.1029/2018JC014137

Donelan, M. A., Drennan, W. M., & Katsaros, K. B. (1997). The air–sea momentum flux in conditions of wind sea and swell. *Journal of Physical Oceanography*, *27*(10), 2087–2099. https://doi.org/10.1175/1520-0485(1997)027<2087:Tasmfi>2.0.Co;2

Drennan, W. M., Graber, H. C., Hauser, D., & Quentin, C. (2003). On the wave age dependence of wind stress over pure wind seas. *Journal of Geophysical Research*, *108*(C3), 8062. https://doi.org/10.1029/2000JC000715

Edson, J. B., Jampana, V., Weller, R. A., Bigorre, S. P., Plueddemann, A. J., Fairall, C. W., et al. (2013). On the exchange of momentum over the open ocean. *Journal of Physical Oceanography*, *43*(8), 1589–1610. https://doi.org/doi:10.1175/jpo-d-12-0173.1

Fairall, C. W., Bariteau, L., Grachev, A. A., Hill, R. J., Wolfe, D. E., Brewer, W. A., et al. (2006). Turbulent bulk transfer coefficients and ozone deposition velocity in the International Consortium for Atmospheric Research into Transport and Transformation. *Journal of Geophysical Research*, *111*, D23S20. https://doi.org/10.1029/2006JD007597

Fairall, C. W., Bradley, E. F., Hare, J. E., Grachev, A. A., & Edson, J. B. (2003). Bulk parameterization of air–sea fluxes: Updates and verification for the COARE algorithm. *Journal of Climate*, *16*(4), 571–591. https://doi.org/10.1175/1520-0442(2003)016<0571:Bpoasf>2.0.Co;2

García-Nava, H., Ocampo-Torres, F. J., Hwang, P. A., & Osuna, P. (2012). Reduction of wind stress due to swell at high wind conditions. *Journal of Geophysical Research*, *117*, C00J11. https://doi.org/10.1029/2011JC007833

García-Nava, H., Ocampo-Torres, F. J., Osuna, P., & Donelan, M. A. (2009). Wind stress in the presence of swell under moderate to strong wind conditions. *Journal of Geophysical Research*, *114*, C12008. https://doi.org/10.1029/2009JC005389

Geernaert, G. L. (1988). Measurements of the angle between the wind vector and wind stress vector in the surface layer over the North Sea. *Journal of Geophysical Research*, *93*(C7), 8215–8220. https://doi.org/10.1029/JC093iC07p08215

Grachev, A., & Fairall, C. (2001). Upward momentum transfer in the marine boundary layer. *Journal of Physical Oceanography*, *31*(7), 1698–1711. https://doi.org/10.1175/1520-0485(2001)031<1698:UMTITM>2.0.CO;2

Grachev, A. A., Bariteau, L., Fairall, C. W., Hare, J. E., Helmig, D., Hueber, J., & Lang, E. K. (2011). Turbulent fluxes and transfer of trace gases from ship-based measurements during TexAQS 2006. *Journal of Geophysical Research*, *116*, D13110. https://doi.org/10.1029/2010JD015502

Grachev, A. A., Fairall, C. W., Hare, J. E., Edson, J. B., & Miller, S. D. (2003). Wind stress vector over ocean waves. *Journal of Physical Oceanography*, *33*(11), 2408–2429. https://doi.org/10.1175/1520-0485(2003)033<2408:Wsvoow>2.0.Co;2

Grare, L., Lenain, L., & Melville, W. K. (2013). Wave-coherent airflow and critical layers over ocean eaves. *Journal of Physical Oceanography*, *43*(10), 2156–2172. https://doi.org/10.1175/jpo-d-13-056.1

Guan, C., & Xie, L. (2004). On the linear parameterization of drag coefficient over sea surface. *Journal of Physical Oceanography*, *34*(12), 2847–2851. https://doi.org/10.1175/jpo2664.1

Hanley, K. E., & Belcher, S. E. (2008). Wave-driven wind jets in the marine atmospheric boundary layer. *Journal of the Atmospheric Sciences*, *65*(8), 2646–2660. https://doi.org/10.1175/2007jas2562.1

Hanley, K. E., Belcher, S. E., & Sullivan, P. P. (2010). A global climatology of wind–wave interaction. *Journal of Physical Oceanography*, *40*(6), 1263–1282. https://doi.org/10.1175/2010jpo4377.1

Harris, D. L. (1966). The Wave-Driven Wind. *Journal of the Atmospheric Sciences*, *23*(6), 688–693. https://doi.org/10.1175/1520-0469(1966)023<0688:Twdw>2.0.Co;2

Högström, U., Rutgersson, A., Sahlée, E., Smedman, A.-S., Hristov, T. S., Drennan, W. M., & Kahma, K. K. (2013). Air–sea interaction features in the Baltic Sea and at a Pacific trade-wind site: An inter-comparison study. *Boundary-Layer Meteorology*, *147*(1), 139–163. https://doi.org/10.1007/s10546-012-9776-8

Högström, U., Sahlée, E., Smedman, A.-S., Rutgersson, A., Nilsson, E., Kahma, K. K., & Drennan, W. M. (2015). Surface stress over the ocean in swell-dominated conditions during moderate winds. *Journal of the Atmospheric Sciences*, *72*(12), 4777–4795. https://doi.org/10.1175/jas-d-15-0139.1

Högström, U., Sahlée, E., Smedman, A.-S., Rutgersson, A., Nilsson, E., Kahma, K. K., & Drennan, W. M. (2018). The transition from downward to upward air–sea momentum flux in swell-dominated light wind conditions. *Journal of the Atmospheric Sciences*, *75*(8), 2579–2588. https://doi.org/10.1175/jas-d-17-0334.1

Högström, U., Smedman, A., Sahleé, E., Drennan, W. M., Kahma, K. K., Pettersson, H., & Zhang, F. (2009). The atmospheric boundary layer during swell: A field study and interpretation of the turbulent kinetic energy budget for high wave ages. *Journal of the Atmospheric Sciences*, *66*(9), 2764–2779. https://doi.org/10.1175/2009jas2973.1

Holthuijsen, L. H., Powell, M. D., & Pietrzak, J. D. (2012). Wind and waves in extreme hurricanes. *Journal of Geophysical Research*, *117*, C09003. https://doi.org/10.1029/2012JC007983

Hristov, T., & Ruiz-Plancarte, J. (2014). Dynamic balances in a wavy boundary layer. *Journal of Physical Oceanography*, *44*(12), 3185–3194. https://doi.org/doi:10.1175/jpo-d-13-0209.1

Hristov, T. S., Miller, S. D., & Friehe, C. A. (2003). Dynamical coupling of wind and ocean waves through wave-induced air flow. *Nature*, *422*(6927), 55–58. https://doi.org/10.1038/nature01382

Jiang, Q., Sullivan, P., Wang, S., Doyle, J., & Vincent, L. (2016). Impact of swell on air-sea momentum flux and marine boundary layer under low-wind conditions. *Journal of the Atmospheric Sciences*, *73*(7), 2683–2697. https://doi.org/10.1175/JAS-D-15-0200.1

Kahma, K. K., Donelan, M. A., Drennan, W. M., & Terray, E. A. (2016). Evidence of energy and momentum flux from swell to wind. *Journal of Physical Oceanography*, *46*(7), 2143–2156. https://doi.org/10.1175/jpo-d-15-0213.1

Kihara, N., Hanazaki, H., Mizuya, T., & Ueda, H. (2007). Relationship between airflow at the critical height and momentum transfer to the traveling waves. *Physics of Fluids*, *19*(1), 015102. https://doi.org/10.1063/1.2409736

Liu, B., Guan, C., & Xie, L. (2012). The wave state and sea spray related parameterization of wind stress applicable from low to extreme winds. *Journal of Geophysical Research*, *117*, C00J22. https://doi.org/10.1029/2011JC007786

Mahrt, L., Miller, S., Hristov, T., & Edson, J. (2018). On estimating the surface wind stress over the sea. *Journal of Physical Oceanography*, *48*(7), 1533–1541. https://doi.org/10.1175/jpo-d-17-0267.1

Mahrt, L., Vickers, D., Sun, J., Jensen, N. O., Jørgensen, H., Pardyjak, E., & Fernando, H. J. B.-L. M. (2001). Determination of the surface drag coefficient. *Boundary-Layer Meteorology*, *99*(2), 249–276. https://doi.org/10.1023/a:1018915228170

Monin, A. S., & Yaglom, A. M. (1971). *Statistical fluid mechanics*, (Vol. 1). Cambridge, Mass: MIT Press.

Nilsson, E. O., Rutgersson, A., Smedman, A.-S., & Sullivan, P. P. (2012). Convective boundary-layer structure in the presence of wind-following swell. *Quarterly Journal of the Royal Meteorological Society*, *138*(667), 1476–1489. https://doi.org/10.1002/qj.1898

Pan, J., Wang, D. W., & Hwang, P. A. (2005). A study of wave effects on wind stress over the ocean in a fetch-limited case. *Journal of Geophysical Research*, *110*, C02020. https://doi.org/10.1029/2003JC002258

Rieder, K. F., & Smith, J. A. (1998). Removing wave effects from the wind stress vector. *Journal of Geophysical Research*, *103*(C1), 1363–1374. https://doi.org/10.1029/97JC02571

Semedo, A., Saetra, Ø., Rutgersson, A., Kahma, K. K., & Pettersson, H. (2009). Wave-induced wind in the marine boundary layer. *Journal of the Atmospheric Sciences*, *66*(8), 2256–2271. https://doi.org/10.1175/2009jas3018.1

Sjöblom, A., & Smedman, A.-S. (2004). Comparison between eddy-correlation and inertial dissipation methods in the marine atmospheric surface layer. *Boundary-Layer Meteorology*, *110*(2), 141–164. https://doi.org/10.1023/a:1026006402060

Smedman, A., Högström, U., Sahleé, E., Drennan, W. M., Kahma, K. K., Pettersson, H., & Zhang, F. (2009). Observational study of marine atmospheric boundary layer characteristics during swell. *Journal of the Atmospheric Sciences*, *66*(9), 2747–2763. https://doi.org/10.1175/2009jas2952.1

Smith, S. D. (1980). Wind stress and heat flux over the ocean in Gale force winds. *Journal of Physical Oceanography*, *10*(5), 709–726. https://doi.org/10.1175/1520-0485(1980)010<0709:Wsahfo>2.0.Co;2

Smith, S. D., Anderson, R. J., Oost, W. A., Kraan, C., Maat, N., De Cosmo, J., et al. (1992). Sea surface wind stress and drag coefficients: The hexos results. *Boundary-Layer Meteorology*, *60*(1-2), 109–142. https://doi.org/10.1007/bf00122064

Soloviev, Y. P., & Kudryavtsev, V. N. (2010). Wind-speed undulations over swell: Field experiment and interpretation. *Boundary-Layer Meteorology*, *136*(3), 341–363. https://doi.org/10.1007/s10546-010-9506-z

Song, J., Fan, W., Li, S., & Zhou, M. (2015). Impact of surface waves on the steady near-surface wind profiles over the ocean. *Boundary-Layer Meteorology*, *155*(1), 111–127. https://doi.org/10.1007/s10546-014-9983-6

Sullivan, P. P., Edson, J. B., Hristov, T., & McWilliams, J. C. (2008). Large-eddy simulations and observations of atmospheric marine boundary layers above nonequilibrium surface waves. *Journal of the Atmospheric Sciences*, *65*(4), 1225–1245. https://doi.org/10.1175/2007jas2427.1

Sullivan, P. P., McWilliams, J. C., & Moeng, C.-H. (2000). Simulation of turbulent flow over idealized water waves. *Journal of Fluid Mechanics*, *404*, 47–85. https://doi.org/doi:10.1017/S0022112099006965

Sullivan, P. P., McWilliams, J. C., & Patton, E. G. (2014). Large-Eddy Simulation of marine atmospheric boundary layers above a spectrum of moving waves. *Journal of the Atmospheric Sciences*, *71*(11), 4001–4027. https://doi.org/10.1175/jas-d-14-0095.1

Takagaki, N., Komori, S., Suzuki, N., Iwano, K., Kuramoto, T., Shimada, S., et al. (2012). Strong correlation between the drag coefficient and the shape of the wind sea spectrum over a broad range of wind speeds. *Geophysical Research Letters*, *39*, L23604. https://doi.org/10.1029/2012GL053988

Vickers, D., Mahrt, L., & Andreas, E. L. (2013). Estimates of the 10-m neutral sea surface drag coefficient from aircraft eddy-covariance measurements. *Journal of Physical Oceanography*, *43*(2), 301–310. https://doi.org/10.1175/jpo-d-12-0101.1

Vickers, D., Mahrt, L., & Andreas, E. L. (2015). Formulation of the sea surface friction velocity in terms of the mean wind and bulk stability. *Journal of Applied Meteorology and Climatology*, *54*(3), 691–703. https://doi.org/10.1175/jamc-d-14-0099.1

Wu, J. (1980). Wind-stress coefficients over sea surface near neutral conditions—A revisit. *Journal of Physical Oceanography*, *10*(5), 727–740. https://doi.org/10.1175/1520-0485(1980)010<0727:Wscoss>2.0.Co;2

Wu, L., Hristov, T., & Rutgersson, A. (2018). Vertical profiles of wave-coherent momentum flux and velocity variances in the marine atmospheric boundary layer. *Journal of Physical Oceanography*, *48*(3), 625–641. https://doi.org/10.1175/jpo-d-17-0052.1

Wu, L., Rutgersson, A., & Nilsson, E. (2017). Atmospheric boundary layer turbulence closure scheme for wind-following swell conditions. *Journal of the Atmospheric Sciences*, *74*(7), 2363–2382. https://doi.org/10.1175/jas-d-16-0308.1

Young, I. R. (2006). Directional spectra of hurricane wind waves. *Journal of Geophysical Research*, *111*, C08020. https://doi.org/10.1029/2006JC003540

Zhang, F. W., Drennan, W. M., Haus, B. K., & Graber, H. C. (2009). On wind-wave-current interactions during the Shoaling Waves Experiment. *Journal of Geophysical Research*, *114*, C01018. https://doi.org/10.1029/2008JC004998

Zou, Z., Zhao, D., Liu, B., Zhang, J. A., & Huang, J. (2017). Observation-based parameterization of air-sea fluxes in terms of wind speed and atmospheric stability under low-to-moderate wind conditions. *Journal of Geophysical Research: Oceans*, *122*, 4123–4142. https://doi.org/10.1002/2016JC012399

Zou, Z., Zhao, D., Zhang, J. A., Li, S., Cheng, Y., Lv, H., & Ma, X. (2018). The influence of swell on the atmospheric boundary layer under nonneutral conditions. *Journal of Physical Oceanography*, *48*(4), 925–936. https://doi.org/10.1175/jpo-d-17-0195.1